JACS
JOURNAL OF THE AMERICAN CHEMICAL SOCIETY
pubs.acs.org/JACS
Communication

Record Quantum Tunneling Time in an Air-Stable Exchange-Bias Dysprosium Macrocycle

Zhenhua Zhu, Sagar Paul,* Chen Zhao, Jianfeng Wu, Xu Ying, Liviu Ungur,* Wolfgang Wernsdorfer, Franc Meyer, and Jinkui Tang*

Cite This: J. Am. Chem. Soc. 2024, 146, 18899−18904
Read Online
ACCESS | Metrics & More | Article Recommendations | Supporting Information

ABSTRACT: In recent years, dysprosium macrocycle single-molecule magnets (SMMs) have received increasing attention due to their excellent air/thermal stability, strong magnetic anisotropy, and rigid molecular skeleton. However, they usually display fast zero-field quantum tunneling of the magnetization (QTM) rate, severely hindering their data storage applications. Herein, we report the design, synthesis, and characterization of an air-stable monodecker didysprosium macrocycle integrating strong single-ion anisotropy, near-perfect local crystal field (CF) symmetry, and efficient exchange bias. These indispensable features enable clear-cut elucidation of the crucial role of very weak antiferromagnetic coupling on magnetization dynamics, creating a prominent SMM with a large effective energy barrier (U_{eff}) of 670 cm^{-1}, open hysteresis loops at zero field up to 14.9 K, and a record relaxation time of QTM (τ_{QTM}), 24281 s, for all known nonradical-bridged lanthanide SMMs.

In the field of lanthanide single-molecule magnets (SMMs), understanding the relationship between the effective energy barrier (U_{eff}) and the blocking temperature (T_B) is key to designing and constructing high-temperature SMMs.[1−3] Numerous lanthanide SMMs with large U_{eff} values have been designed according to the Oblate−Prolate Model due to the electrostatic nature of 4f−ligand interactions.[4,5] However, the development of T_B lags far behind U_{eff} as the former is a more informational metric involving all demagnetization pathways.[6−8] Therefore, generally, improving T_B is more challenging than increasing U_{eff}. Although T_B is governed by complicated spin dynamics,[9] the first step toward high-temperature SMMs is undoubtedly the suppression of the zero-field quantum tunneling of the magnetization (QTM) process. Previous studies have clearly shown that strong intramolecular exchange interactions between different spin centers can strongly mitigate QTM rate and increase T_B.[3,10−15] One of the most typical examples is lanthanide-radical compounds with the general composition of $[\{(Cp^R)_2Ln\}_n(\mu\text{-radical})]$ (n = 2−4) (Cp^R = substituted cyclopentadienyl ligands) where the radical ligand with S = 1/2 possesses a rather diffuse singly occupied molecular orbital that can strongly interact with 4f electrons.[16−20] Recently, Long et al. reported the limiting case of this family, a mixed-valence didysprosium complex, $(Cp^{iPr5})_2Dy_2I_3$ (Figure 1A), in which the two Dy(III) ions are glued by the unpaired electron forming unique Ln−Ln metal bonding.[21] It showed an enormous coercive magnetic field exceeding 14 T at 60 K, which has caught up with commercial permanent magnets.

In spite of the exceptional SMM behaviors of the above lanthanide metallocenes, their extreme sensitivity to air limits their use in molecular devices. In recent years, research has also focused on air-stable species, especially Dy(III)-based macrocyclic compounds.[22−25] However, these compounds typically exhibit evident zero-field QTM behavior. Given that engineering the strong orbital exchange in lanthanide macrocycles is quite difficult,[15,26] it is a promising strategy to consider utilizing dipole coupling to induce exchange biasing. In 2022, we reported a pair of OH^--bridged double-decker dysprosium enantiomers featuring ferromagnetic dipolar coupling.[27] However, the hysteresis loops at zero field are closed as the intramolecular f−f interactions cannot compensate for the weakening of the axial crystal field (CF). Recently, some of us reported a compartmental bis(pyrazolato) bridged macrocycle derived from [2 + 2] condensation of 1,1′-(4-methyl-1*H*-pyrazole-3,5-diyl)bis(ethan-1-one) and 2,2′-diamino-*N*-methyldiethylamine, L^1, that can encapsulate two lanthanide ions into a pentagonal bipyramid environment favoring a dipolar interaction.[28] However, crucial magnetic axiality is absent in the prepared compounds. These works inspire us to construct an air-stable species that possesses strong axiality, high local symmetry, and efficient dipolar coupling simultaneously, which is undoubtedly challenging for synthesis. Here, we report a near-perfect monodecker didysprosium macrocycle, $Dy_2(L^1)$-$(L^2)_4$ (L^2 = 4-(methylthio)phenolate, **Dy_2**, Figure 1B), that fulfills the above three requirements. It is a strong SMM at zero field with U_{eff} of 670 cm^{-1} and open hysteresis loops up to 14.9 K. More impressively, the zero-field relaxation time of QTM (τ_{QTM}) reaches up to 24281 s.

As expected, **Dy_2** is quite robust, with a high thermal decomposition temperature approaching 400 °C (Figure S1). The measured powder X-ray diffraction (PXRD) pattern

Received: May 31, 2024
Revised: July 3, 2024
Accepted: July 3, 2024
Published: July 8, 2024

https://doi.org/10.1021/jacs.4c07412
J. Am. Chem. Soc. 2024, 146, 18899−18904

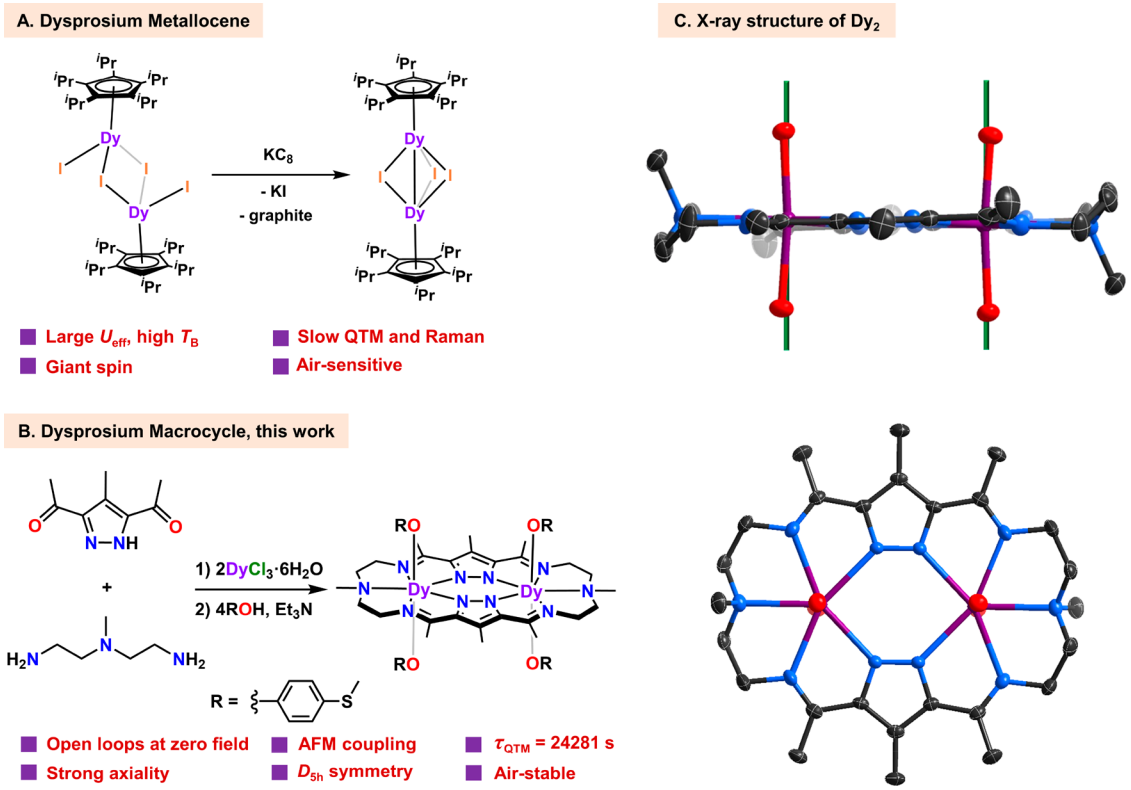

Figure 1. Synthetic routes for $(Cp^{iPr5})_2Dy_2I_3$[21] (A) and **Dy_2** (B). (C) Solid structure of **Dy_2**. The green lines represent the local magnetic axis of the Dy(III) ion from the *ab initio* calculations. Purple, Dy(III); blue, N; red, O; black, C. Hydrogen atoms and axial parts, except for coordinated O_{phen} atoms, are omitted for clarity.

shows good agreement with the simulated one, confirming the pure phase of the sample (Figure S2). Single crystal X-ray analysis revealed that **Dy_2** crystallizes in the monoclinic $P2_1/n$ space group (Table S1) and the two Dy(III) ions in **Dy_2** are bridged by four nitrogen atoms from two pyrazolates with a Dy···Dy distance of 4.779 Å (Figure 1C). Every Dy(III) ion is seven-coordinate and located in a compressed pentagonal-bipyramidal coordination environment (Table S7). The axial phenolate ligands provide relatively short Dy−O distances of 2.1474(18) and 2.1512(18) Å and an almost linear axial O−Dy−O angle of 173.24(7)° (Tables S3−S4). The equatorial macrocycle affords a longer Dy−N distance, averaged to 2.496 Å. In addition, two magnetically diluted samples, **Dy_2@Y_2** and **DyY** with 5% Dy(III), were also prepared for comparative studies according to the reported method (for structural details of **Y_2** see Tables S2, S5, S6, and S8).[29]

The $\chi_M T$ value at 300 K of **Dy_2** is 27.14 cm^3 K mol^{-1} (Figure S4), which is close to the theoretical value of 28.34 cm^3 K mol^{-1} for the two free Dy(III) ions. With decreasing temperatures, the product $\chi_M T$ decreases gradually, followed by a sharp decline at approximately 8 K, which may be due to (i) the progressive depopulation of excited Stark sublevels, (ii) intramolecular antiferromagnetic (AFM) coupling, and (iii) strong magnetic anisotropy. The field dependence of the magnetization was also measured at 1.9, 3.0, and 5 K, giving rise to saturation values of 9.98, 9.95, and 9.89 μ_B at 7 T, respectively, implying that each Dy(III) ion has a strong axiality with $m_J = \pm 15/2$, $g_{eff,z} = 20.0$ (Figure S5). Open magnetic hysteresis loops at zero field were observed between 1.9 and 14.9 K (Figure 2). Comparing the hysteresis loops of **DyY** and **Dy_2@Y_2** (Figure 2, bottom), we can conclude that it is the intramolecular magnetic coupling that shifts the fast QTM away from zero-field and induces open loops.

In the 1.0 to 1500 Hz frequency range, the out-of-phase components of the ac susceptibility (χ'') exhibit well-defined peaks between 20 and 61 K (Figure 3, top). The Cole−Cole plots were obtained from these data and fitted to the generalized Debye model to extract relaxation times (τ) and relaxation distribution (α) (Figure S6 and Table S9). When the temperatures are below 15 K, the magnetic relaxation is too slow to display a maximum even at 0.1 Hz (Figure S7). Consequently, variable-temperature dc magnetization decay experiments were performed to determine τ (Figures S8−S14, and Table S10). In the temperature range of 2−67 K, the plot of ln τ versus T^{-1} is composed of a linear and a slightly curving part, corresponding to the Orbach and Raman relaxation process, respectively (Figure 3, bottom inset). Fitting the data to the equation $\ln(\tau) = -\ln[\tau_0^{-1} \exp(-U_{eff}/k_BT) + CT^n]$ gives $U_{eff} = 670(36)$ cm^{-1}, $\tau_0 = 10^{-10.8(3)}$, $C = 1.42(27) \times 10^{-5}$, $n = 4.63(7)$ with adjusted $R^2 = 0.998$. Based on this plot, we extracted τ_{100s} at 4.1 K.

To obtain information about QTM, we further explored magnetization decay at sub-Kelvin temperatures using μ-SQUIDs (Figure S15 and Table S11). As shown in Figure S16, using the equation $\ln(\tau) = -\ln[(1/10^{p_2}) \exp(-E_2/k_BT) + 1/\tau_{QTM}]$, an excellent fit (adjusted $R^2 = 0.997$) was obtained with $E_2 = 0.36(2)$ K, $p_2 = 3.36(4)$, and $\tau_{QTM} = 24281(709)$ s. To the best of our knowledge, this τ_{QTM} is the largest value for all nonradical-bridged lanthanide SMMs (Table S12). The value of p_2 is comparable to the reported values for magnetically coupled Ln SMMs with bistable ferromagnetic (FM) or AFM ground states.[30] Finally, we extrapolated eq 1 to the entire

https://doi.org/10.1021/jacs.4c07412
J. Am. Chem. Soc. 2024, 146, 18899−18904

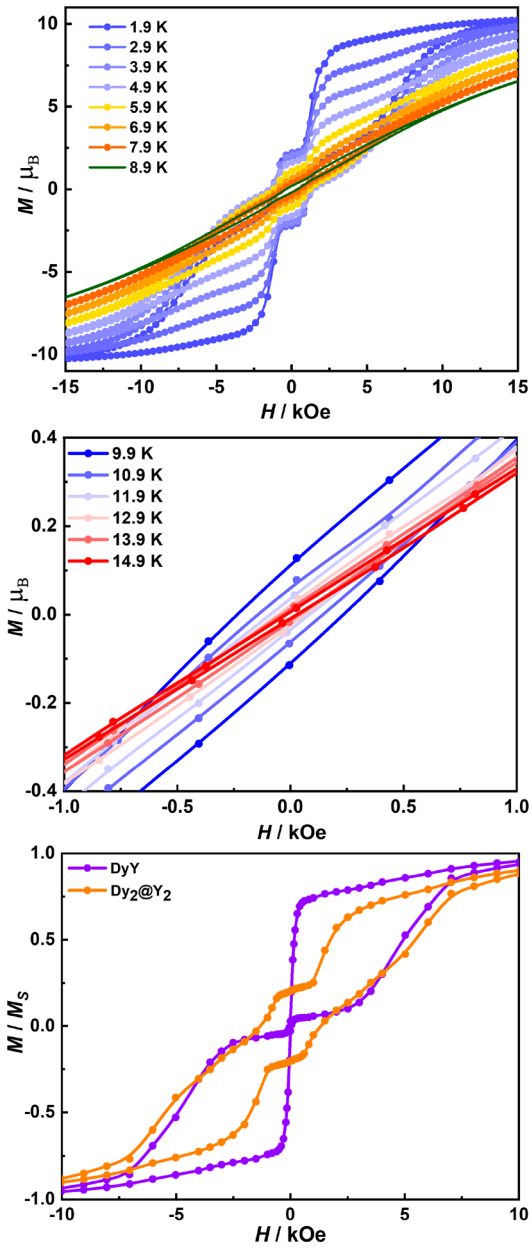

Figure 2. Magnetic hysteresis loops for $\mathbf{Dy_2}$ at a field sweep rate of 200 Oe/s (top and middle). Isothermal magnetization of $\mathbf{Dy_2@Y_2}$ and **DyY** at 1.9 K was obtained for an average sweep rate of 22 Oe/s (bottom).

temperature range, showing an excellent fit quality (Figure 3, bottom). Alternating current measurements on the **DyY** sample were performed to reveal the role of intramolecular magnetic coupling in magnetization dynamics. In the 0.1 to 1500 Hz range, $\chi''(\nu)$ plots exhibited frequency-dependent peaks from 3 to 61 K (Figure S17). The plot of $\ln(\tau)$ against T^{-1} presented a clear plateau at low temperatures with a QTM rate much faster than that in $\mathbf{Dy_2}$. The relaxation rate for **DyY** is fitted by eq 2, giving $U_{\text{eff}} = 648(64)$ cm^{-1}, $\tau_0 = 10^{-10.6(4)}$, $C = (7.4 \pm 2.9) \times 10^{-4}$, $n = 3.56(11)$, and $\tau_{\text{QTM}} = 1.63(25)$ s (Figure S18).

$$\ln(\tau) = -\ln[\tau_0^{-1}\exp(-U_{\text{eff}}/k_{\text{B}}T) + CT^n + (1/10^{p_2})\exp(-E_2/k_{\text{B}}T) + 1/\tau_{\text{QTM}}] \quad (1)$$

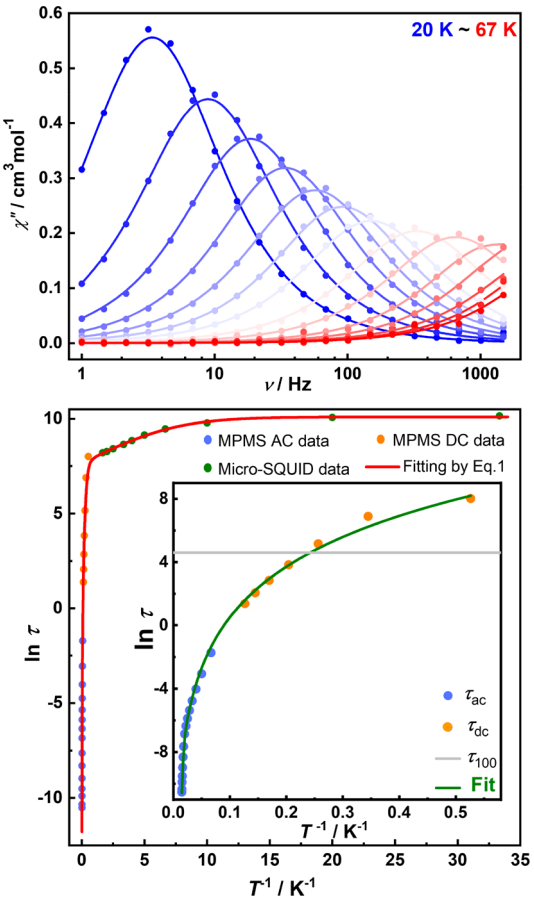

Figure 3. (Top) $\chi''(\nu)$ plots for $\mathbf{Dy_2}$ at a zero applied dc field. The circles and solid lines represent experimental data and fits, respectively. (Bottom) Temperature dependence of the relaxation time τ for $\mathbf{Dy_2}$ and (bottom inset) enlarged view of the same for temperatures above 2 K.

$$\ln(\tau) = -\ln[\tau_0^{-1}\exp(-U_{\text{eff}}/k_{\text{B}}T) + CT^n + 1/\tau_{\text{QTM}}] \quad (2)$$

Magnetic hysteresis curves for a single crystal of $\mathbf{Dy_2}$ were also measured by μ-SQUIDs with the field applied along the easy axis of the crystal (Figure 4 and Figure S19).[31] The hysteresis loops of $\mathbf{Dy_2}$ exhibited an S-shape, typical of antiferromagnetically coupled lanthanide dimers. The measurements also clearly reveal the exchange-bias characteristic of the system with QTM shifting from zero field to 0.1−0.2 T.[32] Magnetic interaction between two axial Dy(III) ions in $\mathbf{Dy_2}$ can be written in terms of the Ising Hamiltonian: $\hat{H}_{\text{exch}} = -J_{\text{Ising}}\tilde{s}_{1z}\tilde{s}_{2z}$, where $\tilde{s}_{1z} = \tilde{s}_{2z} = 1/2$ are the pseudospins of the ground KD on each Dy site. The coupling strength, J_{Ising}, can be calculated using $J_{\text{Ising}} = -4\mu_{\text{B}}g_J m_J H_{\text{ex}}$ with $H_{\text{ex}} = 0.15$ T, $m_J = 15/2$, $g_J = 4/3$, giving $J_{\text{Ising}} = -2.801$ cm^{-1} (see the details in SI). Additionally, μ-SQUID results show interesting details in the low-temperature hysteresis curves: (i) four steps at ±0.15 and ±0.2 T due to the presence of two kinds of macrocyclic planes in the unit cell (Figure S3), confirmed by the angular dependence of $dM/dH(H)$ (Figure S19 bottom); (ii) increasing width of hysteresis loops with increasing T from 30 mK to 2.5 K, indicating more molecules are available in the FM state for the relaxation to the AFM state as temperature is increased in this regime.

Ab initio calculations were carried out to gain further insight into magnetic anisotropy and the relaxation mechanism of

https://doi.org/10.1021/jacs.4c07412
J. Am. Chem. Soc. 2024, 146, 18899−18904

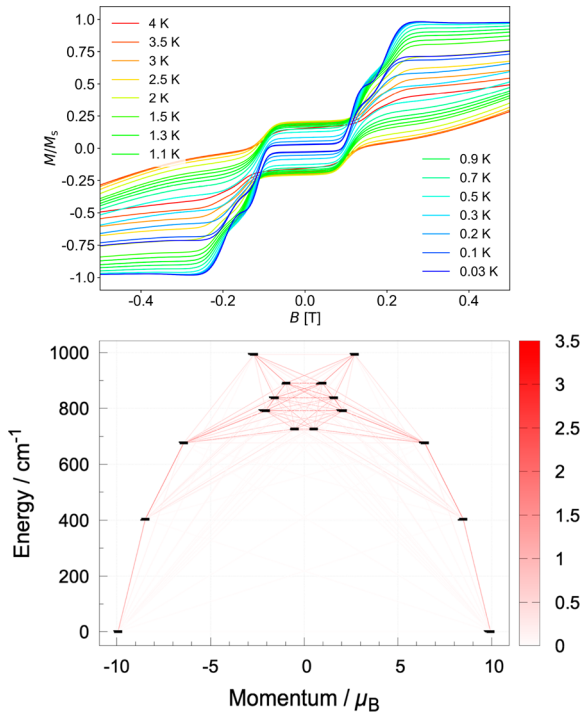

Figure 4. (Top) μ-SQUID measurements on a single crystal of $\mathbf{Dy_2}$ at a constant field sweep rate of 80 Oe/s. (Bottom) Magnetization blocking barriers for an individual Dy site in $\mathbf{Dy_2}$, using the VDZP results.

magnetization.[33,34] As shown in Table S13, the ground Kramers doublets (KDs) of a single Dy(III) site possess a large g_z value, tending to 20.0. The axial CF parameter B_2^0 is negative and larger than any other parameter (Table S14), demonstrating the strong axiality in $\mathbf{Dy_2}$. As expected, the orientation of the ground-state anisotropy axis is directed by the axial phenolate ligand (Figure 1C and Figure S20). For the first excited KDs, the g_z value is also large, approaching 17.0; meanwhile, the transverse components, g_x and g_y, are relatively small, ca. 0.01, which suggests that KD2 is also highly axial. However, for KD3, g_x and g_y significantly increase, leading to less pronounced axiality. Table S15 shows that KD1 and KD2 were assigned to a nearly pure projection of M_J, $\pm 15/2$, and $\pm 13/2$, respectively, while KD3 was composed of mixed wave functions defined by $\pm 11/2$ and $\pm 9/2$. Therefore, the barrier is most likely crossed at KD3 through an Orbach process, giving a calculated U_{eff} of 676 cm^{-1} with VDZP basis sets, which is in excellent agreement with the experimental value. The intramolecular magnetic exchange was evaluated by a broken-symmetry DFT method offering very similar values of about -1.3 to -1.7 cm^{-1} (Table S16), for several exchange functionals. The pure exchange coupling within $\mathbf{Dy_2}$ was also evaluated by fitting the measured magnetic susceptibility using POLY_ANISO,[35] giving the parameter of -0.89 cm^{-1} (Figures S21) for the Ising Hamiltonian presented above. The magnetic dipole−dipole interaction was evaluated using the on-site *ab initio* data, evaluated to -1.559 cm^{-1}. As such, the parameter of total magnetic interaction, -2.45 cm^{-1}, is very close to that determined by μ-SQUID, suggesting that a dominant dipolar coupling induces exchange biasing. From the spectrum of the low-lying exchange multiplets (Table S17), the energy gap between the lowest two exchanged KDs was determined to be 1.225 cm^{-1}, which is sufficient to suppress the QTM process.[36]

To summarize, we designed and prepared an air-stable monodecker didysprosium macrocycle that is a strong SMM at zero field with U_{eff} of 670 cm^{-1}, T_B of 14.9 K, and that features τ_{QTM} up to 24281 s, which is a record value for all known nonradical-bridged lanthanide SMMs. Introducing 4-(methylthio)phenolate generates strong magnetic anisotropy and may also allow monolayer deposition on the gold surface by a strong Au−S bond in the future. The equatorial pyrazole-involved Schiff-base macrocycle ensures near-perfect CF symmetry and efficient exchange biasing, primarily induced by direct dipolar coupling. We need to highlight that the combination of strong single-ion magnetic anisotropy and near-perfect local CF symmetry provides the opportunity to observe the vital role of such weak AFM coupling in the magnetization dynamics.

■ ASSOCIATED CONTENT

Supporting Information

The Supporting Information is available free of charge at https://pubs.acs.org/doi/10.1021/jacs.4c07412.

Experimental details and crystal and magnetic property data (PDF)

Accession Codes

CCDC 2223798 and 2284417 contain the supplementary crystallographic data for this paper. These data can be obtained free of charge via www.ccdc.cam.ac.uk/data_request/cif, or by emailing data_request@ccdc.cam.ac.uk, or by contacting The Cambridge Crystallographic Data Centre, 12 Union Road, Cambridge CB2 1EZ, UK; fax: +44 1223 336033.

■ AUTHOR INFORMATION

Corresponding Authors

Sagar Paul − *Physikalisches Institut, Karlsruhe Institute of Technology (KIT), D-76131 Karlsruhe, Germany;* orcid.org/0000-0001-8317-5778; Email: sagar.paul@kit.edu

Liviu Ungur − *Department of Chemistry, National University of Singapore, Singapore 117543, Singapore;* orcid.org/0000-0001-5015-4225; Email: chmlu@nus.edu.sg

Jinkui Tang − *State Key Laboratory of Rare Earth Resource Utilization, Changchun Institute of Applied Chemistry, Chinese Academy of Sciences, Changchun 130022, P. R. China; School of Applied Chemistry and Engineering, University of Science and Technology of China, Hefei 230026, P. R. China;* orcid.org/0000-0002-8600-7718; Email: tang@ciac.ac.cn

Authors

Zhenhua Zhu − *State Key Laboratory of Rare Earth Resource Utilization, Changchun Institute of Applied Chemistry, Chinese Academy of Sciences, Changchun 130022, P. R. China*

Chen Zhao − *State Key Laboratory of Rare Earth Resource Utilization, Changchun Institute of Applied Chemistry, Chinese Academy of Sciences, Changchun 130022, P. R. China*

Jianfeng Wu − *School of Chemistry and Chemical Engineering, Northwestern Polytechnical University, Xi'an 710072, P. R. China;* orcid.org/0000-0001-6318-1142

Xu Ying − *State Key Laboratory of Rare Earth Resource Utilization, Changchun Institute of Applied Chemistry,*

Chinese Academy of Sciences, Changchun 130022, P. R. China

Wolfgang Wernsdorfer − *Physikalisches Institut, Karlsruhe Institute of Technology (KIT), D-76131 Karlsruhe, Germany;* orcid.org/0000-0003-4602-5257

Franc Meyer − *Institut für Anorganische Chemie, Universität Göttingen, D-37077 Göttingen, Germany;* orcid.org/0000-0002-8613-7862

Complete contact information is available at: https://pubs.acs.org/10.1021/jacs.4c07412

Notes

The authors declare no competing financial interest.

■ ACKNOWLEDGMENTS

This work was supported by the National Natural Science Foundation of China (92261103 and 22201279), the Key Research Program of Frontier Sciences, CAS (ZDBSLY-SLH023). W.W. thanks the German Research Foundation (DFG) concerning the Gottfried Wilhelm Leibniz-Award, ZVN-2020_WE 4458-5. L.U. acknowledges the financial support of the research projects A-8000017-00-00, A-8001894-00-00, and A-8000709-00-00 of the National University of Singapore. *Ab initio* calculations were done on the ASPIRE-2A cluster (www.nscc.sg) under the project 11001278. We thank Dr. Eufemio Moreno-Pineda (PHI, KIT) for the fruitful discussion.

■ REFERENCES

(1) Woodruff, D. N.; Winpenny, R. E. P.; Layfield, R. A. Lanthanide Single-Molecule Magnets. *Chem. Rev.* **2013**, *113*, 5110−5148.

(2) Guo, F.-S.; Bar, A. K.; Layfield, R. A. Main Group Chemistry at the Interface with Molecular Magnetism. *Chem. Rev.* **2019**, *119*, 8479−8505.

(3) Zhu, Z.; Tang, J. Metal-metal bond in lanthanide single-molecule magnets. *Chem. Soc. Rev.* **2022**, *51*, 9469−9481.

(4) Rinehart, J. D.; Long, J. R. Exploiting single-ion anisotropy in the design of f-element single-molecule magnets. *Chem. Sci.* **2011**, *2*, 2078−2085.

(5) Gould, C. A.; McClain, K. R.; Yu, J. M.; Groshens, T. J.; Furche, F.; Harvey, B. G.; Long, J. R. Synthesis and Magnetism of Neutral, Linear Metallocene Complexes of Terbium(II) and Dysprosium(II). *J. Am. Chem. Soc.* **2019**, *141*, 12967−12973.

(6) Castro-Alvarez, A.; Gil, Y.; Llanos, L.; Aravena, D. High performance single-molecule magnets, Orbach or Raman relaxation suppression? *Inorg. Chem. Front.* **2020**, *7*, 2478−2486.

(7) Briganti, M.; Santanni, F.; Tesi, L.; Totti, F.; Sessoli, R.; Lunghi, A. A Complete Ab Initio View of Orbach and Raman Spin-Lattice Relaxation in a Dysprosium Coordination Compound. *J. Am. Chem. Soc.* **2021**, *143*, 13633−13645.

(8) Zhu, Z.; Tang, J. Lanthanide single-molecule magnets with high anisotropy barrier: where to from here? *Natl. Sci. Rev.* **2022**, *9*, nwac194.

(9) Kragskow, J. G. C.; Mattioni, A.; Staab, J. K.; Reta, D.; Skelton, J. M.; Chilton, N. F. Spin-phonon coupling and magnetic relaxation in single-molecule magnets. *Chem. Soc. Rev.* **2023**, *52*, 4567−4585.

(10) Rinehart, J. D.; Fang, M.; Evans, W. J.; Long, J. R. Strong exchange and magnetic blocking in N_2^{3-}-radical-bridged lanthanide complexes. *Nat. Chem.* **2011**, *3*, 538−542.

(11) Liu, F.; Spree, L.; Krylov, D. S.; Velkos, G.; Avdoshenko, S. M.; Popov, A. A. Single-Electron Lanthanide-Lanthanide Bonds Inside Fullerenes toward Robust Redox-Active Molecular Magnets. *Acc. Chem. Res.* **2019**, *52*, 2981−2993.

(12) Liu, X.; Feng, X.; Meihaus, K. R.; Meng, X.; Zhang, Y.; Li, L.; Liu, J.-L.; Pedersen, K. S.; Keller, L.; Shi, W.; Zhang, Y.-Q.; Cheng, P.; Long, J. R. Coercive Fields Above 6 T in Two Cobalt(II)-Radical Chain Compounds. *Angew. Chem., Int. Ed.* **2020**, *59*, 10610−10618.

(13) Velkos, G.; Krylov, D. S.; Kirkpatrick, K.; Spree, L.; Dubrovin, V.; Büchner, B.; Avdoshenko, S. M.; Bezmelnitsyn, V.; Davis, S.; Faust, P.; Duchamp, J.; Dorn, H. C.; Popov, A. A. High Blocking Temperature of Magnetization and Giant Coercivity in the Azafullerene $Tb_2@C_{79}N$ with a Single-Electron Terbium-Terbium Bond. *Angew. Chem., Int. Ed.* **2019**, *58*, 5891−5896.

(14) Wang, Y.; Velkos, G.; Israel, N. J.; Rosenkranz, M.; Büchner, B.; Liu, F.; Popov, A. A. Electrophilic Trifluoromethylation of Dimetallofullerene Anions en Route to Air-Stable Single-Molecule Magnets with High Blocking Temperature of Magnetization. *J. Am. Chem. Soc.* **2021**, *143*, 18139−18149.

(15) Xin, J.; Hu, Z.; Yao, Y. R.; Ullah, A.; Han, X.; Xiang, W.; Jin, H.; Jiang, Z.; Yang, S. Short Didysprosium Covalent Bond Enables High Magnetization Blocking Temperature of a Direct 4f-4f Coupled Dinuclear Single-Molecule Magnet. *J. Am. Chem. Soc.* **2024**, *146*, 17600.

(16) Demir, S.; Jeon, I.-R.; Long, J. R.; Harris, T. D. Radical ligand-containing single-molecule magnets. *Coord. Chem. Rev.* **2015**, *289*−*290*, 149−176.

(17) Demir, S.; Zadrozny, J. M.; Nippe, M.; Long, J. R. Exchange Coupling and Magnetic Blocking in Bipyrimidyl Radical-Bridged Dilanthanide Complexes. *J. Am. Chem. Soc.* **2012**, *134*, 18546−18549.

(18) Gould, C. A.; Mu, E.; Vieru, V.; Darago, L. E.; Chakarawet, K.; Gonzalez, M. I.; Demir, S.; Long, J. R. Substituent Effects on Exchange Coupling and Magnetic Relaxation in 2,2'-Bipyrimidine Radical-Bridged Dilanthanide Complexes. *J. Am. Chem. Soc.* **2020**, *142*, 21197−21209.

(19) Demir, S.; Gonzalez, M. I.; Darago, L. E.; Evans, W. J.; Long, J. R. Giant coercivity and high magnetic blocking temperatures for N_2^{3-} radical-bridged dilanthanide complexes upon ligand dissociation. *Nat. Commun.* **2017**, *8*, 2144.

(20) Zhang, P.; Luo, Q.-C.; Zhu, Z.; He, W.; Song, N.; Lv, J.; Wang, X.; Zhai, Q.-G.; Zheng, Y.-Z.; Tang, J. Radical-Bridged Heterometallic Single-Molecule Magnets Incorporating Four Lanthanoceniums. *Angew. Chem., Int. Ed.* **2023**, *62*, No. e202218540.

(21) Gould, C. A.; McClain, K. R.; Reta, D.; Kragskow, J. G. C.; Marchiori, D. A.; Lachman, E.; Choi, E.-S.; Analytis, J. G.; Britt, R. D.; Chilton, N. F.; Harvey, B. G.; Long, J. R. Ultrahard magnetism from mixed-valence dilanthanide complexes with metal-metal bonding. *Science* **2022**, *375*, 198−202.

(22) Canaj, A. B.; Dey, S.; Martí, E. R.; Wilson, C.; Rajaraman, G.; Murrie, M. Insight into D_{6h} Symmetry: Targeting Strong Axiality in Stable Dysprosium(III) Hexagonal Bipyramidal Single-Ion Magnets. *Angew. Chem., Int. Ed.* **2019**, *58*, 14146−14151.

(23) Zhu, Z.; Zhao, C.; Feng, T.; Liu, X.; Ying, X.; Li, X.-L.; Zhang, Y.-Q.; Tang, J. Air-Stable Chiral Single-Molecule Magnets with Record Anisotropy Barrier Exceeding 1800 K. *J. Am. Chem. Soc.* **2021**, *143*, 10077−10082.

(24) Gil, Y.; Castro-Alvarez, A.; Fuentealba, P.; Spodine, E.; Aravena, D. Lanthanide SMMs Based on Belt Macrocycles: Recent Advances and General Trends. *Chem.—Eur. J.* **2022**, *28*, No. e202200336.

(25) Corredoira-Vázquez, J.; González-Barreira, C.; Oreiro-Martínez, P.; García-Deibe, A. M.; Sanmartín-Matalobos, J.; Fondo, M. Synthesis and applications of lanthanoid complexes of pentadentate and hexadentate N_5 and N_6 macrocycles: A review. *J. Rare Earths* **2024**, *42*, 1−15.

(26) Morita, T.; Damjanović, M.; Katoh, K.; Kitagawa, Y.; Yasuda, N.; Lan, Y.; Wernsdorfer, W.; Breedlove, B. K.; Enders, M.; Yamashita, M. Comparison of the Magnetic Anisotropy and Spin Relaxation Phenomenon of Dinuclear Terbium(III) Phthalocyaninato Single-Molecule Magnets Using the Geometric Spin Arrangement. *J. Am. Chem. Soc.* **2018**, *140*, 2995−3007.

(27) Zhu, Z.; Zhao, C.; Zhou, Q.; Liu, S.; Li, X.-L.; Mansikkamäki, A.; Tang, J. Air-Stable Dy(III)-Macrocycle Enantiomers: From Chiral to Polar Space Group. *CCS Chem.* **2022**, *4*, 3762−3771.

(28) Wu, J.; Demeshko, S.; Dechert, S.; Meyer, F. Macrocycle based dinuclear dysprosium(III) single molecule magnets with local D_{5h} coordination geometry. *Dalton Trans.* **2021**, *50*, 17573−17582.
(29) Habib, F.; Lin, P.-H.; Long, J.; Korobkov, I.; Wernsdorfer, W.; Murugesu, M. The Use of Magnetic Dilution To Elucidate the Slow Magnetic Relaxation Effects of a Dy_2 Single-Molecule Magnet. *J. Am. Chem. Soc.* **2011**, *133*, 8830−8833.
(30) Orlova, A. P.; Hilgar, J. D.; Bernbeck, M. G.; Gembicky, M.; Rinehart, J. D. Intuitive Control of Low-Energy Magnetic Excitations via Directed Dipolar Interactions in a Series of Er(III)-Based Complexes. *J. Am. Chem. Soc.* **2022**, *144*, 11316−11325.
(31) Wernsdorfer, W.; Chakov, N. E.; Christou, G. Determination of the magnetic anisotropy axes of single-molecule magnets. *Phys. Rev. B* **2004**, *70*, 132413.
(32) Wernsdorfer, W.; Aliaga-Alcalde, N.; Hendrickson, D. N.; Christou, G. Exchange-biased quantum tunnelling in a supramolecular dimer of single-molecule magnets. *Nature* **2002**, *416*, 406.
(33) Aquilante, F.; Autschbach, J.; Carlson, R. K.; Chibotaru, L. F.; Delcey, M. G.; De Vico, L.; Fdez. Galván, I.; Ferré, N.; Frutos, L. M.; Gagliardi, L.; Garavelli, M.; Giussani, A.; Hoyer, C. E.; Li Manni, G.; Lischka, H.; Ma, D.; Malmqvist, P. Å.; Müller, T.; Nenov, A.; Olivucci, M.; Pedersen, T. B.; Peng, D.; Plasser, F.; Pritchard, B.; Reiher, M.; Rivalta, I.; Schapiro, I.; Segarra-Martí, J.; Stenrup, M.; Truhlar, D. G.; Ungur, L.; Valentini, A.; Vancoillie, S.; Veryazov, V.; Vysotskiy, V. P.; Weingart, O.; Zapata, F.; Lindh, R. Molcas 8: New capabilities for multiconfigurational quantum chemical calculations across the periodic table. *J. Comput. Chem.* **2016**, *37*, 506−541.
(34) Fdez. Galván, I.; Vacher, M.; Alavi, A.; Angeli, C.; Aquilante, F.; Autschbach, J.; Bao, J. J.; Bokarev, S. I.; Bogdanov, N. A.; Carlson, R. K.; Chibotaru, L. F.; Creutzberg, J.; Dattani, N.; Delcey, M. G.; Dong, S. S.; Dreuw, A.; Freitag, L.; Frutos, L. M.; Gagliardi, L.; Gendron, F.; Giussani, A.; González, L.; Grell, G.; Guo, M.; Hoyer, C. E.; Johansson, M.; Keller, S.; Knecht, S.; Kovačević, G.; Källman, E.; Li Manni, G.; Lundberg, M.; Ma, Y.; Mai, S.; Malhado, J. P.; Malmqvist, P. Å.; Marquetand, P.; Mewes, S. A.; Norell, J.; Olivucci, M.; Oppel, M.; Phung, Q. M.; Pierloot, K.; Plasser, F.; Reiher, M.; Sand, A. M.; Schapiro, I.; Sharma, P.; Stein, C. J.; Sørensen, L. K.; Truhlar, D. G.; Ugandi, M.; Ungur, L.; Valentini, A.; Vancoillie, S.; Veryazov, V.; Weser, O.; Wesołowski, T. A.; Widmark, P.-O.; Wouters, S.; Zech, A.; Zobel, J. P.; Lindh, R. OpenMolcas: From Source Code to Insight. *J. Chem. Theory Comput.* **2019**, *15*, 5925−5964.
(35) Chibotaru, L. F.; Ungur, L.; Soncini, A. The Origin of Nonmagnetic Kramers Doublets in the Ground State of Dysprosium Triangles: Evidence for a Toroidal Magnetic Moment. *Angew. Chem., Int. Ed.* **2008**, *47*, 4126−4129.
(36) Bernbeck, M. G.; Orlova, A. P.; Hilgar, J. D.; Gembicky, M.; Ozerov, M.; Rinehart, J. D. Dipolar Coupling as a Mechanism for Fine Control of Magnetic States in ErCOT-Alkyl Molecular Magnets. *J. Am. Chem. Soc.* **2024**, *146*, 7243−7256.

https://doi.org/10.1021/jacs.4c07412
J. Am. Chem. Soc. 2024, 146, 18899−18904